

Document downloaded from:

<http://hdl.handle.net/10251/150321>

This paper must be cited as:

Carpio-Cobo, P.; Candidato, RTJ.; Pawlowski, L.; Salvador Moya, MD. (2019). Solution concentration effect on mechanical injection and deposition of YSZ coatings using the solution precursor plasma spraying. *Surface and Coatings Technology*. 371:124-130.
<https://doi.org/10.1016/j.surfcoat.2018.10.088>



The final publication is available at

<https://doi.org/10.1016/j.surfcoat.2018.10.088>

Copyright Elsevier

Additional Information

Solution concentration effect on mechanical injection and deposition of YSZ coatings using the solution precursor plasma spraying

**Pablo Carpio^{1,2,*}, Rolando T. Candidato, Jr.³, Lech Pawłowski¹, María Dolores
Salvador²**

1 – Institut de Recherche sur les Céramiques (IRCER), UMR 7315 CNRS, Université de Limoges. 12 rue Atlantis 87068, Limoges, France

2 - Instituto de Tecnología de Materiales (ITM), Universitat Politècnica de València, Valencia.
Cami de Vera s/n 46022, Valencia, Spain

3 - Department of Physics, MSU-Iligan Institute of Technology, A. Bonifacio Avenue,
Tibanga, 9200, Iligan City, Philippines

* **Corresponding author:** Pablo Carpio

Address: Instituto de Tecnología de Materiales (ITM). Ciutat Politècnica de la Innovació, ed 8B semisótano, Cami de Vera s/n, 46022, Valencia, Spain.

Tel. number: (+34) 660806113

Fax number: (+34) 963877629

Email address: pabcarco@upv.es

ABSTRACT

YSZ coatings were developed by solution precursor plasma spraying from different solution concentrations. The solutions were characterized and correlated with the rheological properties (specific weight, viscosity and surface tension). The mechanical injection was used therefore a correct injection is essential to get a correct liquid jet break-up inside the plasma plume. The optimal injection pressure must be adjusted for each solution since the solution characteristics affect on the injection process. It was experimentally found out by the observation of the splats' morphology. The particles were not melted at low pressures but solidified prior to the deposition when the injection pressure is high. It was also found out that the optimal static pressure varies with the concentration, but the dynamic pressure is equal for every solutions and slightly superior to the dynamic pressure of the plasma plume. After injection optimization, coatings using different solution concentrations were developed and their microstructures were investigated. The liquid jet fragmentations as well as the heat requirements were modified with the concentration so that coating microstructure was affected. The resulting coatings display a lamellar and porous microstructure with the presence of unmelted/unpyrolysed material. Coatings' porosity increased while coatings' grow-up was less intensive when diluted solutions were used as feedstock.

KEYWORDS: Solution precursor plasma spraying; Yttria-stabilized zirconia; Thermal barrier coating

1. Introduction

Finely-structured materials have been extensively studied in the last years because they exhibit improved features comparing with their conventional counterparts. Atmospheric plasma spraying (APS) is a suitable technique to deposit thick ceramic coatings but one of its limitations is the deposition of fine particles. Coatings from fine particles improve the characteristics respect to their conventional counterparts but particles smaller than 20 μm cannot be injected because of their low density and poor flowability [1]. In order to solve this problem, some modifications have been realized and some new techniques such as suspension plasma spraying (SPS) and solution precursor plasma spraying (SPPS) were developed[2–4]. The main characteristic of these techniques consists of using the liquid feedstock injection (suspension or solution precursor) instead of a powder. Two possible mechanisms have been developed to inject liquids: spray atomization and mechanical injection. The atomization needs an external energy (centrifugal force, external pressure kinetic energy of another fluid, etc.) to break up the liquid jet, and the atomized liquid is injected inside the plasma plume where a secondary break up occurs due to the high drag forces between the droplet and the plasma. In a mechanical injection, the liquid feedstock is forced to drive through a nozzle by a pressurized system. In this case, the secondary break up which occurs inside the plasma plume is crucial in the formation of the droplets. Immediately after the fragmentation, a series of phenomena as the solvent evaporation, the pyrolysis in the case of SPPS deposition, and the solid melting occur inside the plasma jet. The droplet size, energy requirements and the heat transfer control the described phenomena.

SPPS deposition has been studied to develop different kinds of application such as solid oxide fuel cells [5], bioactive coatings [6,7], sensors [8,9] and etc. It exhibits some advantages with respect to SPS, i.e. molecular level mixing of constituent chemicals, quick chemical formulation, or the control of amount of unpyrolyzed material [10]. One of the most studied

coating material has been the yttria-stabilized zirconia (YSZ) for thermal barrier applications because of its low thermal conductivity and good stability at high temperature [10–12].

Some aspects of the SPPS deposition have been treated in several works. Concretely, the effect of spraying parameters in the coating microstructure, and consequently the coating properties, has been extensively studied [13–15]. Besides the influence of the feedstock (precursor chemistry, solvent type, concentration...) has been also studied since the liquid jet fragmentation, energy requirements or the heat transfer between feedstock and plasma plume are modified [16–18]. However, the variation of the injection process in function of the change of feedstock properties has not been considered in the case of the mechanical injection. An appropriate correct solution injection is crucial element of deposition process since the liquid jet must enter inside the plume core. The liquid injection depends on the specific weight and speed of the plasma gases and the liquid jet. Hence the injection speed must be adjusted for each solution since its density and other properties changes as discussed by various authors such as e.g. [2,3].

The liquid feedstock can be injected inside the plasma plume by two different modes: mechanical and atomization. A primary break-up of the liquid jet occurs outside the plasma plume in the case of atomization mode, and then the droplets are injected inside the plume and a secondary break-up can occur because of the high kinetic energy of the plasma. Although Chen et al. [16] addressed the effect of the concentration on the splat morphology and on the coating microstructure but the atomization was used as injection mechanism and the feedstock flow rate and the fragmentation jet was controlled by the atomizing gas. In the case of the mechanical injection, the flow rate and the jet diameter was adjusted by the static pressure and the nozzle diameter respectively. Besides, a primary fragmentation did not occur and consequently, the secondary fragmentation, which depends on the injection, became primary. Hence, a correct injection displays a higher importance in the case of mechanical injection.

A study was performed in the present work to inject correctly the precursor solutions with different concentrations by means of mechanical injection system. It was realized by adjusting the feedstock flow rate. YSZ coatings obtained from solutions at different concentrations were compared and their microstructures were discussed considering the processes which occur inside the plasma jet.

2. Experimentation

2.1. Preparation of the precursors and its characterization

The precursors used as feedstocks were zirconium acetate ($\text{Zr}[\text{C}_2\text{H}_3\text{O}_2]_4$) and yttrium nitrate $\text{Y}[\text{NO}_3]_4$, both supplied by Sigma Aldrich, USA. They were mixed using a magnetic stirrer for 1 hour in a stoichiometric ratio corresponding to 4 wt.% yttria-stabilized zirconia. The precursors were diluted at different ratios to study the effect of the feedstock concentration in the spraying process. The dilutions were performed with a mixture of ethanol and water 50/50 wt. %. The previous research work reported that this mixture is optimal [19].

The solution precursor plasma spraying used in this work is a complex process, where the in-flight phenomena experienced by solution droplets affect considerably the final microstructural characteristics of the coatings. Moreover, the phase transitions and possible formation of decomposition phases as well as other reaction by-products may occur and should be characterized and associated to the phase composition of the coatings. In order to observe the thermal behavior of the precursors vs. temperature, they were tested by thermogravimetric analysis and differential scanning analysis (TG-DTA) with the use of *STA 449 F3 Jupiter* (Netzsch, Germany). The dried precursor was placed in an alumina crucible and was heated from 25 °C to 900 °C with a heating rate of 10 °C/min under argon atmosphere. The crystalline phases of the precursors treated at different temperatures were also found by X-ray diffraction (D8 Advance, Brucker, USA) under Bragg-Brentano configuration with $\text{Cu K}_{\alpha 1}=0.15406 \text{ nm}$

radiation. A step increment of 0.02° (θ) in the scanning range of 20° – 80° (θ) was used and the resulting diffractogram was analyzed using *Diffrac + EVA Software*. Prior to thermal characterization of the precursors, they were dried at $150\text{ }^\circ\text{C}$ in an electrical furnace, being the weight loss around 5%, and a amorphous solid is obtained after the drying. The thermal treatments at different temperatures were realized in an electric furnace with a 1h of dwell time and slow cooling.

The rheological behavior of the precursors with different concentrations was determined using a rotational rheometer (RheolabQC, Anton Paar, Austria) operating at controlled shear rate (CR) by loading the shear rate from 0 to 1000 s^{-1} in 300 s, maintaining at 1000 s^{-1} for 60 s and downloading from 1000 to 0 s^{-1} in 300 s. The measurements were carried out at $25\text{ }^\circ\text{C}$ using a double-gap cylinder system since this geometry is optimal for the measurement of low viscous liquids [20]. Surface tension was measured by tensiometer (DCAT11, DataPhysics Instruments, Germany) using a platinum Wilhelmy plate system.

2.2. Plasma spray process

Coatings were deposited using a single cathode plasma torch (SG-100, Praxair, USA) mounted on a 5-axis robot (IRB-6, ABB, Switzerland). The liquid feedstock was injected by mechanical system which consists of two pressurized vessels (one for the feedstock and the other one for the water), connected to one nozzle of 0.3 mm diameter located radially at 8 mm from the exit of the plasma plume and with an angle of 30° . The static pressure inside the vessels can be controlled and it results is crucial in the injection optimization as well as the control of the feedstock flow rate. The injection was external since corrosion problems in the torch were observed using the internal injection.

The splats morphology at different static pressures and solution molarities was evaluated. For this purpose, polished stainless steel (AISI 316L) substrates were used and one scan with a high

torch scanning speed (1000 mm/s) was deposited to observe the splats. Then, thick coatings from different solution were developed using the optimal static pressure optimized thanks to the splats observation. Sand-blasted substrates were used for this purpose since a rough surface is necessary to improve the adherence. The number of spraying passes was adapted in each coating to achieve a thickness around 100 μm . The spraying parameters were kept constants for every coating: electrical power of 40 kW, argon and hydrogen as plasma gases with flow rate of 45 slpm and 5 slpm respectively, spraying distance of 60 mm and a torch scan speed of 500 mm/s. The spraying parameters were selected from previous works [21].

2.3 Coating characterization

Splats morphology and coating microstructure (topography and cross-section) were observed by scanning electron microscopy (JEOL IT 300 LV, Jeol Cop, Japan) at low vacuum mode coupled with electron dispersion spectrometer (EDS). The samples were embedded in an epoxy resin and polished up to 0.1 μm to examine the coating cross-section. Besides, the porosity and thickness was calculated by image analysis (Image-Pro Plus, Media Cybernetics, USA) from 10 SEM micrographs at 2000x and 500x magnification respectively. Then, the crystalline phases of the coatings were detected by XRD.

3. Results

3.1 Precursor characterization

Thermal behavior examination of the precursors at equilibrium conditions was conducted to understand the processes which might take place during spraying. Fig.1 shows the thermogram of the dried precursor in which 60% of weight loss was observed over the entire temperature cycle. Two small endothermic points at 125 and 225 °C were observed and attributed to the physically adsorbed water evaporation which corresponds to a loss weight of 16%. However,

the main weight loss is attributed to the chemical reaction decomposition to volatile gases, formation amorphous ZrO₂ and Y₂O₃ as reflected in the exothermic peak at 350°C. The most important exothermic peak is reflected at 500°C which corresponds to the formation of the former ZrO₂ crystals while boarder exothermic peak at 820°C corresponds to the crystalline grown of tetragonal ZrO₂. These findings agree with the literature data [22]. It is important to remark that the YSZ formation is an exothermic process therefore, it means an energetic contribution inside the plasma plume which is beneficial especially in conventional torches where the power is limited.

The crystalline phases formed at different temperatures were confirmed by XRD, as shown in Fig. 2. The dried precursor and precursor treated at low temperatures was amorphous since no crystalline lattice was formed. Some peaks were distinguished at 450 ° and 700 °C of treatment and attributed to YSZ pattern but they are small and broad. This mean that small crystalline nucleus could have been formed but the crystalline lattice is formed at higher temperatures at which the YSZ pattern is clearly observed. Precursor treated at 850°C and 1000°C was tetragonal YSZ (pdf Card No.50-1089) being more crystalline at 1000°C.

The rheological behavior of the precursors diluted at different ratios can be observed in the flow curves (Fig. 3). The relationship between shear rate and shear stress was linear with a correlation R²>0.99. It means that the solutions exhibited a Newtonian behavior with constant viscosity. This result is important in the injection of liquid feedstocks since shear rate in the injector is huge so the viscosity should be low even at high shear rates [23]. The variation of the surface tension and the apparent viscosity at different solution concentration, which affects in the injection and the coating microstructure, is plotted in Fig. 4. It is observable that both surface tension and viscosity are increased when the solution concentration was higher.

3.2 Splat morphology

Single torch scans at different static injection pressures were performed with the aim of finding the optimal injection. For this purpose, the splats morphology for each scan was observed by SEM. It was concluded that the splats morphology depends on the injection pressure rather than the solution concentration. Fig. 5 displays huge difference in the deposits at several static pressures in the case of 4 mol/L solution. At low pressures (60 kPa for 4 mol/l solution), no splats were found and only bulk fragmented solids were observed. These fragmented solids could have corresponded to the big solution droplets whose solvent was evaporated during the spraying but the solid was unmelted. Rounded and flattened particles with the typical spat morphology appeared in the center of the sprayed zone when the static pressure is increased (80 kPa for 4 mol/l solution), although no melted material remains in lower proportion in the edge of the sprayed zone. In the case of very high pressures (higher than 1.0 bar/l solution), rounded and no flatten particles can be observed which seems to be badly adhered. These particles consist ~~pyrolyzed and~~ melted material which solidified before impacting onto the substrate [2,17].

Unmelted material flattened and rounded particles can be observed when different solution concentrations were sprayed at different static pressures. However, the different kind of deposits were observed at different pressures. The pressure necessary to observe the splats changes so that typical splats and resolidified particles were appreciated at lower pressures when the solution concentration was reduced. The static pressure for which the splats were observed without unmelted material was selected as the optimal one [24]. Figure 6 display single scan images of solutions with different n molarity using the optimal pressure. Splats with similar morphology and different sizes (between 2 and 40 μm) were observed and average splat size seems to be reduced at lower concentrations. As the splat size was lower than that obtained at conventional APS coatings and slightly lower than SPS coatings, it can be deduced that the microstructure of these SPPS coatings is finer [1].

3.3 Coating microstructure

The cross-sections micrographs of the coatings (Fig. 7) reveals a bimodal microstructure observed in suspension plasma sprayed coatings [24]. It consists of unmelted or unpyrolyzed material surrounded by a melted matrix having a lamellar microstructure. The porosity of these coatings is high because the unmelted zones retains a high amount of micropores (diameter $< 1 \mu\text{m}$) although some macropores (diameter $> 1 \mu\text{m}$) can be found inside the melted matrix [24]. Transversal cracks were clearly observed just in 4 mol/L coating and some of them in 2 mol/L coating. These cracks are caused by the thermal stresses created during the deposition. Besides, these cracks can improve the thermal fatigue resistance by stress discharge [12].

The porosity and thickness of these coatings are shown in Table 1. The porosity values are high but the coatings are even more porous when the starting solution was diluted. The thickness growth by pass was smaller for low concentration solution. The weight of material sprayed was directly proportional to the solution concentration. It can be deduced that that a higher amount of material gets lost when diluted solutions are sprayed.

Figure 8 shows different coatings' topography. Coatings from concentrated solutions exhibited an almost planar surface with some small clusters. However, bigger clusters appeared at lower molarities, with a cauliflower-type microstructure typical in columnar coatings [25]. Although the columnar structure is not really present in these coatings (some columns were visible in coating sprayed using 0.5 mol/L solution), the formation of columnar microstructure by reduction of the solution concentration confirms the results of previous research [25]. Micrographs at higher magnification revealed that coatings are formed by particles smaller than $1 \mu\text{m}$ (which correspond to the splats) but big agglomerates are also present (which correspond to resolidified material).

XRD patterns of coatings obtained from different solutions are shown in Fig. 9. The patterns are quite similar and just tetragonal phase is observed. Besides, the chemical composition of the coatings, as well as of the splats, is homogeneity since it was corroborated by EDS. Thus, the crystalline phases and chemical composition are independent on solution concentration.

4. Discussion

4.1 Solution injection

Before spraying, the injection is optimized by selection of different static pressures (p_0 , kPa). However, the dynamic pressure (p_k , kPa), is the crucial parameter which influences injection [1,2]. It is defined as:

$$p_k = \rho \cdot v^2 \quad (1)$$

Where ρ is the solution density (kg/m^3) and v is the feedstock injection speed (m/s). The speed was calculated from the feed rate which was experimentally determined:

$$v = \frac{Q}{A} = \frac{M/\rho}{\pi/4D^2} \quad (2)$$

Where Q is the volumetric flow rate (m^3/s), M is the feed rate (kg/s), A is the injector section (m^2) and D is the injector diameter (m). Table 2 shows the flow rate, speed and dynamic pressure of a solution injected at different static pressures. It is clearly seen that these parameters change with static pressure.

According to the literature, the liquid jet can penetrate plasma plume when the dynamic pressure of the liquid jet ($p_{k,l}$) is equal or higher than the dynamic pressure of the plasma plume [1,2].

$$p_{k,l} \geq p_{k,g} \quad (3)$$

Maps of the plasma gas speed and specific weight, and consequently the dynamic pressure, could be calculated using the software T&TWinner [26]. It was found that the maximum dynamic pressure of the plume was 11 kPa. As seen in Table 3, the dynamic pressure of the solution was found to be ~15 kPa in all the cases, which equates to a slightly superior pressure

than the dynamic pressure of the plasma, which was calculated to be 11 kPa as stated before. These findings agree with the literature which addressed that dynamic pressure of the feedstock must be equal or higher than dynamic pressure of the plume [2]. On the other hand, it may happen that for too high liquid jet pressure, the jet goes radially through the plume instead of holding inside the center of plume. This may correspond to the situation of solid which gets pyrolysed and melted inside the plume but resolidifying before impacting onto the substrate. It agrees with the results observed in the Fig. 5. An illustrative diagram of the injection at different pressures is shown in Fig. 10.

The optimal injection pressure is different for each solution, as it was demonstrated in section 3.4. Since the specific weight changes therefore the liquid jet speed must be adjusted. Hence, the feedstock flow rate is modified changing the injection pressure and it must be taken into account in the heat transfer between plasma plume and the feedstock.

4.2 Droplet fragmentation

Coating microstructure depends on the phenomena which occur inside the plasma plume, such us: (i) jet fragmentation; (ii), evaporation solvent; (iii), pyrolysis; and, (iv) solid melting. Thus, it is important to understand the effect of the solution concentration (molarity) in each one of these phenomena. The liquid jet fragmentation is hard to estimate. Nevertheless, the literature correlates the fragmentation with two dimensionless numbers: Weber (*We*) and Ohnersorge (*Oh*):

$$We = \frac{\text{Inertial force}}{\text{Surface tension force}} = \frac{\rho_g(v_g - v_l)^2 d_l}{\sigma_l} \quad (4)$$

$$Oh = \frac{\text{Viscous force}}{\text{Surface tension force}} = \frac{\mu_l}{\sqrt{\rho_l d_l \sigma_l}} \quad (5)$$

Where ρ is the density (kg/m^3), v is the speed (m/s), σ is the surface tension (N/m), μ is the viscosity ($\text{Pa}\cdot\text{s}$) and d_l is the jet diameter (m) considering it is 1.5 times higher nozzle diameter

[2]. Index g and l refers the plasma plume and liquid feedstock respectively. It can be seen in Table 3 that Oh number is almost constant but the Weber number depends on the concentration via surface tension. A stripping break-up occurs at We numbers between 100 -350, but the fragmentation increases with the We values. It means that smaller droplets are formed at lower concentration, therefore, the deposited splats had a reduced size, as can be seen in Fig.10 6.

4.3 Heat transfer

The plasma must provide the heat necessary to evaporate the solvent and to melt the solid in the case of suspensions but the energy delivery or absorbed in the pyrolysis must be also considered. These requirements depend on the feedstock and on the degree of unmelted or unpyrolysed particles in the coatings. As the feedstocks were composed of the precursors such as zirconium acetate and yttrium nitrate delivered heat during its pyrolysis (see Fig. 1). On the other hand, the feedstock contains solvent which must be evaporated prior to the pyrolysis. The specific enthalpy of solvent evaporation (1.78 MJ/kg in the present case) is one order higher than the solid melting. ~~Consequently, the heat needed for evaporation is the greatest one (enthalpy of the solvents is as high as 1.78 MJ/kg)~~. Thus, diluted solutions need more heat because of the higher content of solvent. It can be ~~realled~~ pointed that 4 mol/L solution is almost pure precursor while 0.5 mol/L solution just contain only 12 mass% of it.) and needs less heat for pyrolysis.

Other factor which affects in the required thermal energy is the feedstock flow rate which was smaller at lower concentrations. It reduced the thermal energy needed by 20%, which is relatively small comparing to of the energy needed by solvent to evaporate. The higher thermal energy needed by solution results in the presence of unmelted/unpyrolysed material, as can be observed in Fig. 7 and Table1

Also, heat transfer between the liquid feedstock and the plasma plume must be considered. The transfer depends on the feedstock and on plasma jet properties, as well as, on the droplet size. The heat arrives rapidly to the center of small droplet. At big droplets a solid shell can be formed on the external part since evaporation occurs before the heat necessary to pyrolyze the center of the droplet. The presence of shells in the droplets of concentrated solutions can be correlated with the presence of unpyrolysed material in some coatings [3].

Finally, an effect phenomenon related to the liquid jet fragmentation is the Knudsen effect. The effect results in small droplets moving parallel to the substrate. It may lead to the formation of columns and higher roughness of coatings sprayed using diluted solutions [2], which is demonstrated in the topographic microstructures of Figure 6.

5. Conclusion

YSZ coatings were successfully developed by SPPS process. Firstly, the feedstock characterizations were performed and it was corroborated that rheological properties depends on solution concentration (viscosity and surface tension increase at higher concentrations). Then, the optimal injection pressure was selected from the splat observation. It was important because the feedstock cannot be well-injected at low pressures and mostly unmelted material is deposited. On the other hand, resolidified material (spherical particles instead of flatten drops) can be found at high pressures since jet cross the plasma plume. Thus, the static pressure must be adjusted for each solution since the optimal static pressure depends on the solution characteristics. Finally, solutions of different concentrations were applied to obtain coatings characterized microstructurally. The coatings sprayed using diluted solution exhibited higher porosity and greater content of unmelted zones because of the higher energetic requirement to evaporate the solvent. However, some coatings sprayed using concentrated solution also displayed high porosity since the droplet fragmentation is lower (higher surface tension

therefore lower Weber number). Big droplets mean that a shell is formed in the external part of the droplets during the pyrolysis and it contribute in the porosity retention. It can be concluded that the injection must be adjusted to spray solutions with different concentration in order to obtain desired coatings' microstructure. Besides, it is corroborated that coating microstructure depends on feedstock characteristics as well as the injection process.

Acknowledgment

This work has been supported by the Spanish Ministry of Economy and Competitiveness (project MAT2015-67586-C3-R). P. Carpio acknowledges the Valencia Government (APOSTD/2016/040) and the Spanish Ministry of Science, Innovation and Universities for his current post-doc contract (FJCI-2016-27822) for his post-doc contract.

Reference

- [1] P. Fauchais, G. Montavon, R.S. Lima, B.R. Marple, Engineering a new class of thermal spray nano-based microstructures from agglomerated nanostructured particles, suspensions and solutions: an invited review, *J. Phys. D. Appl. Phys.* 44 (2011) 93001. doi:10.1088/0022-3727/44/9/093001.
- [2] P. Fauchais, A. Joulia, S. Goutier, C. Chazelas, M. Vardelle, A. Vardelle, S. Rossignol, Suspension and solution plasma spraying, *J. Phys. D. Appl. Phys.* 46 (2013). doi:10.1088/0022-3727/46/22/224015.
- [3] L. Pawłowski, Suspension and solution thermal spray coatings, *Surf. Coatings Technol.* 203 (2009) 2807–2829. doi:10.1016/j.surfcoat.2009.03.005.
- [4] A. Killinger, R. Gadow, G. Mauer, A. Guignard, R. Vaen, D. Stöver, Review of new developments in suspension and solution precursor thermal spray processes, *J. Therm. Spray Technol.* 20 (2011) 677–695. doi:10.1007/s11666-011-9639-8.
- [5] Y. Wang, T.W. Coyle, Solution precursor plasma spray of nickel-yittia stabilized zirconia anodes for solid oxide fuel cell application, *J. Therm. Spray Technol.* 16 (2007) 898–904. doi:10.1007/s11666-007-9108-6.
- [6] R.T. Candidato, P. Sokołowski, L. Pawłowski, A. Denoirjean, Preliminary study of hydroxyapatite coatings synthesis using solution precursor plasma spraying, *Surf. Coatings Technol.* 277 (2015) 242–250. doi:10.1016/j.surfcoat.2015.07.046.
- [7] Y. Xiao, L. Song, X. Liu, Y. Huang, T. Huang, J. Chen, Y. Wu, F. Wu, Bioactive glass-ceramic coatings synthesized by the liquid precursor plasma spraying process, *J. Therm. Spray Technol.* 20 (2011) 560–568. doi:10.1007/s11666-010-9594-9.
- [8] C. Zhang, X. Geng, H. Li, P.J. He, M.P. Planche, H. Liao, M.G. Olivier, M. Debliquy, Microstructure and gas sensing properties of solution precursor plasma-sprayed zinc oxide coatings, *Mater. Res. Bull.* 63 (2015) 67–71. doi:10.1016/j.materresbull.2014.11.044.
- [9] K. Chien, T.W. Coyle, Rapid and continuous deposition of porous nanocrystalline SnO₂coating with interpenetrating pores for gas sensor applications, *J. Therm. Spray Technol.* 16 (2007) 886–892. doi:10.1007/s11666-007-9076-x.
- [10] M. Gell, E.H. Jordan, M. Teicholz, B.M. Cetegen, N.P. Padture, L. Xie, D. Chen, X. Ma, J. Roth, Thermal barrier coatings made by the solution precursor plasma spray process, *J. Therm. Spray Technol.* 17 (2008) 124–135. doi:10.1007/s11666-007-9141-5.
- [11] M. Gell, L. Xie, X. Ma, E.H. Jordan, N.P. Padture, Highly durable thermal barrier coatings made by the solution precursor plasma spray process, *Surf. Coatings Technol.* 177–178 (2004) 97–102. doi:10.1016/j.surfcoat.2003.06.023.
- [12] A. Ganvir, N. Curry, S. Govindarajan, N. Markocsan, Characterization of Thermal Barrier Coatings Produced by Various Thermal Spray Techniques Using Solid Powder, Suspension, and Solution Precursor Feedstock Material, *Int. J. Appl. Ceram. Technol.* 13 (2016) 324–332. doi:10.1111/ijac.12472.

- [13] L. Xie, X. Ma, A. Ozturk, E.H. Jordan, N.P. Padture, B.M. Cetegen, D.T. Xiao, M. Gell, Processing parameter effects on solution precursor plasma spray process spray patterns, *Surf. Coatings Technol.* 183 (2004) 51–61. doi:10.1016/j.surfcoat.2003.09.071.
- [14] Y. Wang, T.W. Coyle, Optimization of solution precursor plasma spray process by statistical design of experiment, *J. Therm. Spray Technol.* 17 (2008) 692–699. doi:10.1007/s11666-008-9227-8.
- [15] P. Fauchais, R. Etchart-Salas, V. Rat, J.F. Coudert, N. Caron, K. Wittmann-Ténèze, Parameters controlling liquid plasma spraying: Solutions, sols, or suspensions, *J. Therm. Spray Technol.* 17 (2008) 31–59. doi:10.1007/s11666-007-9152-2.
- [16] D. Chen, E.H. Jordan, M. Gell, The solution precursor plasma spray coatings: Influence of solvent type, *Plasma Chem. Plasma Process.* 30 (2010) 111–119. doi:10.1007/s11090-009-9200-4.
- [17] D. Chen, E.H. Jordan, M. Gell, Effect of solution concentration on splat formation and coating microstructure using the solution precursor plasma spray process, *Surf. Coatings Technol.* 202 (2008) 2132–2138. doi:10.1016/j.surfcoat.2007.08.077.
- [18] W. Duarte, S. Rossignol, M. Vardelle, La₂Zr₂O₇(LZ) Coatings by Liquid Feedstock Plasma Spraying: The Role of Precursors, *J. Therm. Spray Technol.* 23 (2014) 1425–1435. doi:10.1007/s11666-014-0131-0.
- [19] P. Sokołowski, L. Łatka, L. Pawłowski, A. Ambroziak, S. Kozerski, B. Nait-Ali, Characterization of microstructure and thermal properties of YCSZ coatings obtained by suspension plasma spraying, *Surf. Coatings Technol.* 268 (2015) 147–152. doi:10.1016/j.surfcoat.2014.10.006.
- [20] B. Cappi, J. Ebert, R. Telle, Rheological properties of aqueous Si₃N₄ and MoSi₂ suspensions tailor-made for direct inkjet printing, *J. Am. Ceram. Soc.* 94 (2011) 111–116. doi:10.1111/j.1551-2916.2010.04052.x.
- [21] R.T. Candidato, P. Sokołowski, L. Pawłowski, G. Lecomte-Nana, C. Constantinescu, A. Denoirjean, Development of hydroxyapatite coatings by solution precursor plasma spray process and their microstructural characterization, *Surf. Coatings Technol.* 318 (2017) 39–49. doi:10.1016/j.surfcoat.2016.10.072.
- [22] S. Govindarajan, R.O. Dusane, S.V. Joshi, In situ particle generation and splat formation during solution precursor plasma spraying of yttria-stabilized zirconia coatings, *J. Am. Ceram. Soc.* 94 (2011) 4191–4199. doi:10.1111/j.1551-2916.2011.04773.x.
- [23] P. Carpio, M.D. Salvador, A. Borrell, E. Sánchez, R. Moreno, Alumina-zirconia coatings obtained by suspension plasma spraying from highly concentrated aqueous suspensions, *Surf. Coatings Technol.* 307 (2016). doi:10.1016/j.surfcoat.2016.09.060.
- [24] P. Carpio, E. Bannier, M.D. Salvador, A. Borrell, R. Moreno, E. Sánchez, Effect of particle size distribution of suspension feedstock on the microstructure and mechanical properties of suspension plasma spraying YSZ coatings, *Surf. Coatings Technol.* 268 (2015). doi:10.1016/j.surfcoat.2014.08.063.

- [25] P. Sokołowski, S. Kozerski, L. Pawłowski, A. Ambroziak, The key process parameters influencing formation of columnar microstructure in suspension plasma sprayed zirconia coatings, *Surf. Coatings Technol.* 260 (2014) 97–106.
doi:10.1016/j.surfcoat.2014.08.078.
- [26] B. Pateyron, L. Pawłowski, N. Calve, G. Delluc, A. Denoirjean, Modeling of phenomena occurring in plasma jet during suspension spraying of hydroxyapatite coatings, *Surf. Coatings Technol.* 214 (2013) 86–90.
doi:10.1016/j.surfcoat.2012.11.006.

Table list

Table 1. Porosity, thickness and thickness by pass of coatings sprayed at different solution concentrations.

Concentration (mol/L)	Porosity (%)	Thickness (μm)	Thickness/pass (μm)
4	25±4	114±5	14.2
2	26±4	106±4	6.6
1	35±5	96±4	3.0
0.5	34±7	32±5	1.6

Table 2. Flow rate (M: in mass, Q: in volume), speed (v) and dynamic pressure (p_k) of 4 mol/L solution injected at different static pressures (p_0).

p_0 (kPa)	M (g/min)	Q (ml/min)	v (m/s)	P_k (kPa)
60	20.1	14.1	3.33	7.9
80	28.0	19.6	4.63	15.3
100	34.1	23.9	5.64	22.7

Table 3. Flow rate (M: in mass, Q: in volume), speed (v), dynamic pressure (p_k), Weber number (We) and Ohnesorge number (Oh) of different solutions (different molarity and specific weight) injected at optimal static pressure (p_0)..

Molarity (mol(L))	Specific weight (kg/m ³)	p_0 (kPa)	M (g/min)	Q (ml/min)	v (m/s)	p_k (kPa)	We	Oh
4.0	1425	80	28.0	19.6	4.63	15.3	199	0.030
2.0	1153	70	25.0	21.6	5.10	15.0	260	0.031
1.0	1018	60	23.4	23.0	5.42	15.0	305	0.033
0.5	950	50	22.8	24.0	5.66	15.2	321	0.031

Figure captions

Figure 1. DTA-TG diagram of the solution precursor used for the synthesis of 4 mol% YSZ by SPPS (continuous: DTA; striped: TG).

Figure 2. XRD pattern of the precursor used for the synthesis of 4 mol% YSZ by SPPS treated at different temperatures.

Figure 3. Flow curves (shear stress vs shear rate) of precursors diluted at different ratios.

Figure 4. Apparent viscosity (stripped line) and surface tension (continuous line) of the precursors at different concentrations.

Figure 5. Single scan depositions of 4 mol/L solution sprayed at different static pressures: a) 0.6 bar; b) 0.8 bar; c) 1 bar.

Figure 6. Single scan depositions at optimal static pressure (marked between parenthesis) of solutions at different concentration.

Figure 7. Cross-section micrographs of coatings obtained at different solution concentration: left micrographs at 500x; right micrographs at 2500x.

Figure 8. Surface micrographs of coatings obtained at different solution concentration: left micrographs at 200 x; right micrographs at 2000 x.

Figure 9. XRD pattern of the coatings obtained from solutions with different concentrations.

Figure 10. Sketch of the injection and the liquid jet trajectory at different static pressures.

Figure

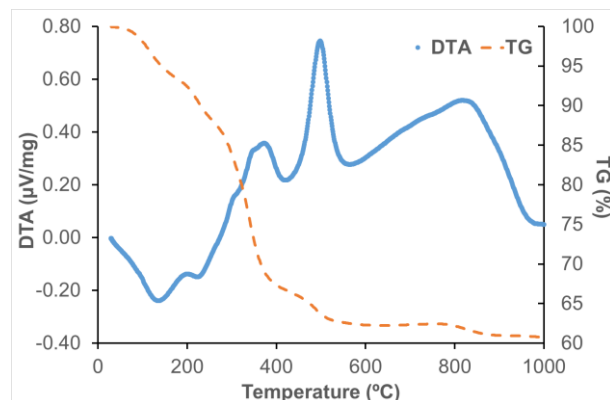


Figure 1

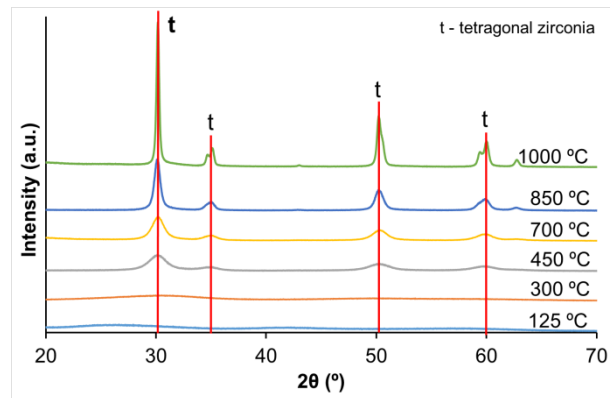


Figure 2

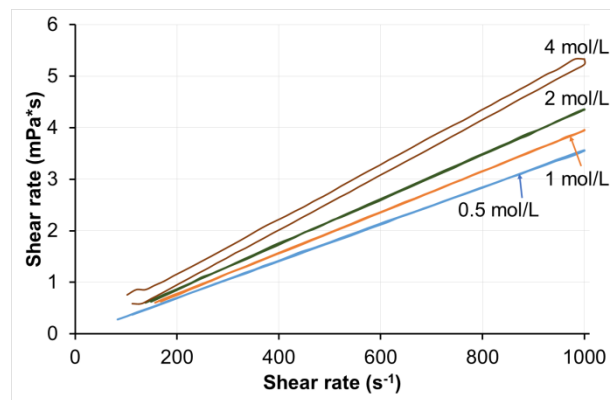


Figure 3

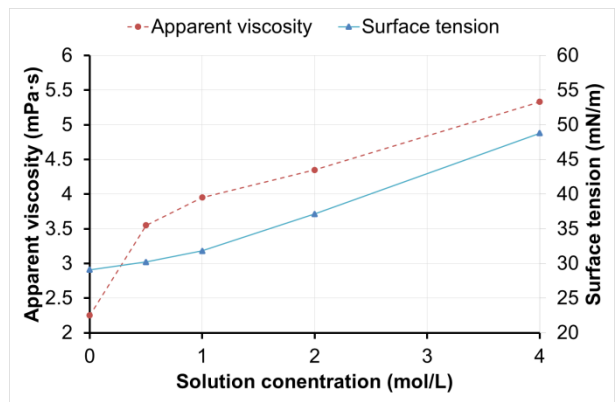


Figure 4

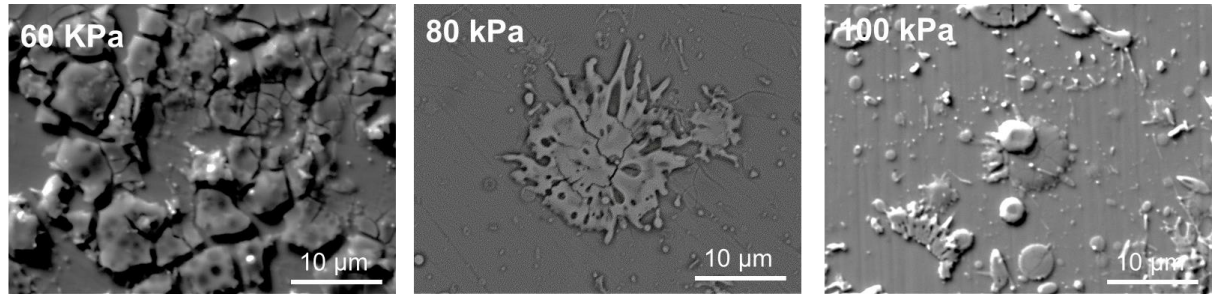


Figure 5

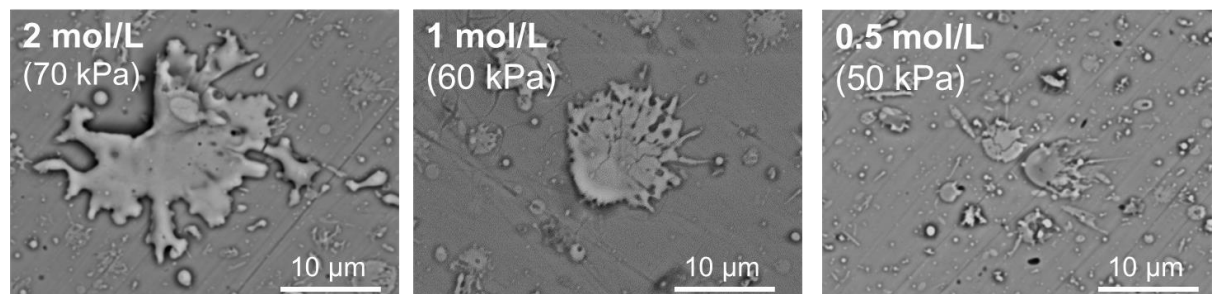


Figure 6

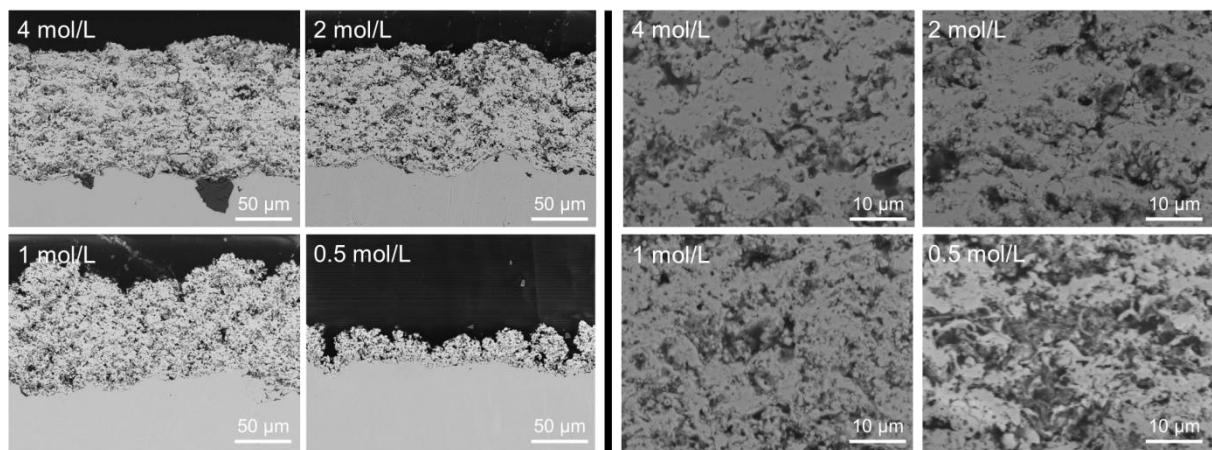


Figure 7

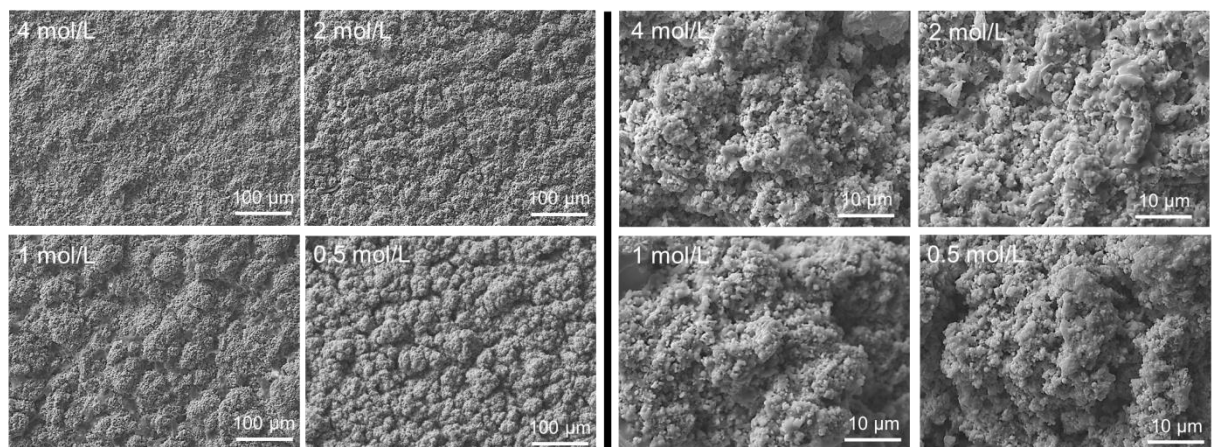


Figure 8

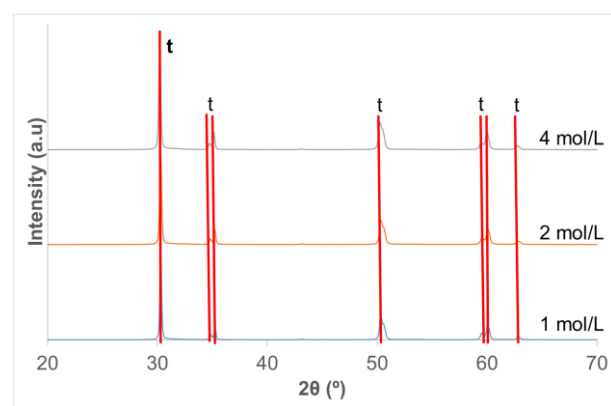


Figure 9

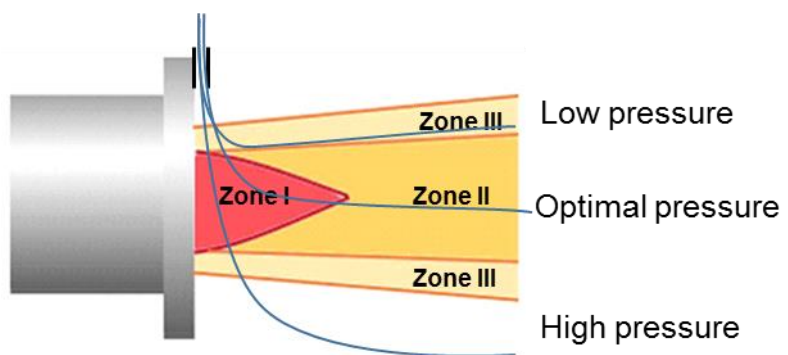


Figure 10